Displacement-threshold energies in Si calculated by molecular dynamics

L. A. Miller
Sandia National Laboratories, P.O. Box 5800, Albuquerque, New Mexico 87185
and Chemical & Nuclear Engineering Department, University of New Mexico, Albuquerque, New Mexico 87131

D. K. Brice
Sandia National Laboratories, P.O. Box 5800, Albuquerque, New Mexico 87185

A. K. Prinja
Chemical & Nuclear Engineering Department, University of New Mexico, Albuquerque, New Mexico 87131

S. T. Picraux
Sandia National Laboratories, P.O. Box 5800, Albuquerque, New Mexico 87185
(Received 28 June 1993; revised manuscript received 2 March 1994)

Molecular-dynamics calculations of simple defect production in bulk Si are reported. The Tersoff three-body potential-energy function is used to provide a realistic lattice-atom interaction potential. The displacement-threshold energy E_d is calculated as a function of the initial primary knock-on momentum direction, and the formation energies for resulting defect structures are obtained. In addition, we determine the effect of the vacancy-interstitial separation on the anisotropy in E_d, where the criterion for stable Frenkel-pair defect formation is assumed to require a certain minimum separation. The resultant angular dependent E_d versus (θ,ϕ) is compared with that proposed by Hemment and Stevens (HS) to account for the magnitude and anisotropy of the observed energetic electron-induced radiation damage in Si. The anisotropy of our E_d surface is consistent with that of HS provided a lower limit of 4 Å is placed on the initial Frenkel-pair separation for the production of long-lived damage. The relatively large formation energy of 8.4 eV which we obtain for such widely separated vacancy-interstitial pairs indicates that the individual point defects are essentially isolated (i.e., noninteracting). More closely spaced vacancy-interstitial complexes are also identified, which have lower formation energies. While it is argued that these complexes are relatively short lived, they may be relevant to dynamical processes such as beam-enhanced molecular-beam epitaxy, atomic mixing at interfaces, and "subthreshold" damage production.

I. INTRODUCTION

Molecular-dynamics (MD) simulations of radiation effects were first used by Vineyard and co-workers in studies of radiation-induced defect production in fcc copper[1] and bcc iron.[2] Similar studies were carried out subsequently for fcc iron by Beeler and Beeler.[3] These investigations were primarily motivated by concerns arising from the radiation-induced damage observed in nuclear-reactor structural materials, and Cu and Fe provided simple model systems for the then available electronic computing machines.

A variety of defects and defect properties in metals have been investigated by application of MD techniques. Defects and their properties that have been addressed include vacancies, divacancies, vacancy migration, vacancy clusters, and self-interstitials in bcc iron, fcc iron, nickel, and hcp metals, as well as the effects of impurity atoms in metal lattices.[4] In related studies, the anisotropy in displacement-threshold energy in Fe (Ref. 3) and Cu (Ref. 5) lattices has been investigated in detail.

These early MD studies were most tractable for metals because of the relatively simple potential functions required to describe the interactions between atoms. In general, pairwise central forces were used, which were supplemented by special "surface" forces on atoms near the boundary of the computational crystal to represent interactions with the surrounding material. The composite potentials used unique functional representations in each of several ranges of the interatomic separation distance, with the parameters adjusted to give agreement with the observed elastic properties, cohesive energies, and minimum displacement-threshold energies. Theoretical estimates were generally used for very small interatomic separations.

In contrast to metals, semiconductors require a more complex potential-energy function to provide for adequate MD simulations. This requirement is due to the highly directional covalent bonding in these materials, which rules out the simple central-force representations used for metals. In addition, torsional effects in semiconductors due to bond overlap lead to three-body forces. In recent years, many potentials that consider these factors have been proposed for silicon, including Stillinger and Weber,[6] (SW), Tersoff,[7–10] Biswas and Hamann,[11] Dodson,[12] and Bolding and Andersen.[13]

One of the earliest potentials proposed was the SW formulation,[6] which adequately modeled the structure of

 ©1994 The American Physical Society

both the crystalline and liquid phases of Si. Other authors have applied the SW potential to a wide range of systems,[14] and have shown this potential function to be quite useful in qualitative studies. The SW potential, however, provides an inadequate description for undercoordinated or overcoordinated Si,[13] and thus is less useful, for example, for surface studies. The Tersoff potential has also been extensively applied to MD studies of Si,[7,8,10] and in particular to surface phenomena.[15] The basic Tersoff form of the potential was also chosen by Bolding and Andersen as the starting point in the development of their potential because of "the generality of the approach and the physical justification for the chosen form."[13] Perhaps the most accurate potential function for Si now available may be that developed by Bolding and Andersen,[13] however, the complexity of this potential, which includes four-body terms, precludes its extensive use in MD calculations at present.

As indicated above, the Tersoff potential has been used extensively in modeling the dynamics of Si surfaces. Particular emphasis has been given to such defect-mediated processes at surfaces as sputtering, surface-adatom migration, and epitaxial growth.[15–18] Recently, beam-enhanced epitaxial growth and doping experiments have motivated detailed MD studies of ion-bombardment-induced Si surface and near-surface (to ≈ 15 layers deep) defect production, configurations, and subsequent stability.[16–18] Other MD calculations focusing on bulk Si have tended to examine the static properties of point defects, for example, vacancy- and interstitial-formation energies. In the present paper we report MD calculations relating to the *dynamics* of bulk-defect formation in Si. In these studies, we focus on the anisotropy in the displacement-threshold energy for Frenkel-pair production. A preliminary account of some of this work has been presented elsewhere.[19]

One key issue in MD studies of displacement thresholds is the precise definition of a displacement event. A simple definition was used in obtaining the results we reported earlier,[19] namely, that the primary knock-on atom (PKA) in the silicon lattice is considered displaced when it exits the tetrahedron formed by the nearest-neighbor atoms and comes into quasithermal equilibrium with the surrounding lattice before recombination can occur. (By quasithermal equilibrium we mean that the total available kinetic energy is more or less randomly distributed over all atoms in the computational cell.) Values for the displacement-threshold energy E_d resulting from this definition were found to be only about 50% of those values deduced from radiation-damage studies using electron bombardment,[20] and a different anisotropy was found as well. Consequently, we have examined the displacement process in more detail and the MD results reported here suggest a "natural" separation for stable Frenkel-pair production. This approach produces much better agreement with experiment and also correctly accounts for the observed anisotropy. In effect, the simple definition of displacement often leads to closely spaced Frenkel pairs, which, we argue, are short lived due to vacancy-interstitial interactions through the crystal-strain field; only widely separated pairs persist for sufficient time to contribute to the observed damage.

The definition of a displacement event is thus found to be dependent on the time scale over which the Frenkel pair exerts its influence on the property being measured. As indicated, for long-term stability our results suggest a large separation. We note, however, that for applications to dynamic processes (e.g., smoothening and roughening of surface growth,[21] atomic mixing at interfaces,[22] ion-bombardment-induced solid-phase epitaxy,[23] and subthreshold damage processes[24]), the simple definition used earlier for the displacement event may also be relevant. In this respect we also note that for none of the MD calculations of point-defect production in metals has this issue been discussed (i.e., the question of defect stability has not been precisely defined in the early studies).

In what follows, we present a description of our molecular-dynamics simulation technique in Sec. II. The MD results are given in Sec. III, and these are discussed in Sec. IV.

II. MOLECULAR-DYNAMICS SIMULATION TECHNIQUE

The molecular-dynamics computer code written for the calculations reported here is based on standard procedures, and thus we briefly highlight only special features of the present algorithm. Atomic positions are initialized in the equilibrium sites of the bulk silicon lattice. In general, the atomic velocities are determined by sampling a Maxwell-Boltzmann distribution corresponding to the desired initial sample temperature. However, in the present study, the initial velocities were set to zero to approximate a zero-temperature crystal. We point out, however, that a significant temperature increase occurs when a test atom (the PKA) is given a kinetic energy near the expected displacement-threshold energy (~ 15 eV). For our standard computational cell size of 576 atoms, a PKA kinetic energy of 15 eV results in a temperature rise of approximately 100–150 K (the lower value corresponds to a displaced atom with a formation energy of approximately 6 eV; the higher temperature corresponds to no displacement).

For the bulk processes described here, periodic boundary conditions were imposed separately on the boundaries in each of the three Cartesian coordinate directions, resulting in the three-dimensional infinite repetition of the computational cell. Here, we use the Tersoff potential,[10] primarily due to the relative simplicity involved in implementing it in our code, but also because the parameter values can be adjusted to describe other diamond-lattice crystals (e.g., C, Ge, SiC). This silicon potential uses Tersoff's latest parameter values, which provide a better description of bond-bending forces than his earlier parametrizations,[7,8] while still providing a satisfactory description of point defects.

The equations of motion are integrated according to a scheme developed by Smith and Harrison.[25] The efficiency of our code is increased by taking advantage of the finite range of the Tersoff potential function, i.e., force calculations are performed only for those atoms separated by less than the potential cutoff distance. The

time increment Δt is calculated at the beginning of each time step. The value of Δt is chosen to be inversely proportional to the speed of the most energetic atom in the computational cell, with a proportionality constant such that this atom moves at most 0.05 A per time step.

Extensive testing of the code was carried out to ensure that the calculation was properly implemented. The cohesive energy predicted by the code for Si of 4.63 eV/atom agrees with the experiment and the Tersoff evaluation, suggesting that we have correctly implemented the potential-energy function. Further, during a 5-ps simulation (typically 1000 time steps), the energy is conserved to better than five significant figures, indicating that we are properly integrating the equations of motion. The results of such calculations are found to be essentially independent of time-step size, and are not significantly altered when utilizing the corrector step of the Smith and Harrison[25] integration scheme (i.e., by increasing the accuracy in the integration procedure). The corrector step was not used in the calculations reported below since it requires two force calculations per time step with a corresponding increase in CPU time to complete a simulation. We did, however, adjust the magnitudes of the atomic velocities after each time step by a multiplicative constant to provide exact conservation of energy, thereby improving the integration procedure.

It became evident that the energy-conserving procedure (ECP) described at the end of the previous paragraph does not enjoy wide application in the MD community. We, therefore, elaborate briefly on the ECP here. A numerical solution to the equations of motion is said to be accurate to $O(t^n)$, where t is the integrator step size, when $R \sim O(t^n)$, where R is the distance in phase space between the points representing the numerical and the exact solutions. Further, it is clear that each point in phase space within a distance R of that representing the exact solution represents an equally valid solution to the equations within the specified accuracy. Some of these points represent solutions that conserve energy; most do not. The solutions that conserve energy have clear benefits in certain types of calculations, e.g., those following a thermally driven process for long integration times, and we think of them as being "more accurate," although technically they are no closer to the exact solution in phase space than those within R, which are energy nonconserving. That our ECP makes a transformation from a nonconservative solution to a conservative solution within R is easily proved from the equations relating total energy to the momenta and coordinates in phase space. We note that the ECP has no substantial effect on the calculations reported here since the integrations span only a few picoseconds, but as indicated above it does offer significant benefits in other types of calculation.

The size of the crystal used in these calculations was $6a$ in the [100], $6a$ in the [010], and $2a$ in the [001], where a is the cubic unit-cell lattice constant (5.43 Å for silicon) for a total of 576 atoms. For each calculation the PKA, which was located at the center of the crystal, was given an initial velocity in the desired direction. These recoil energies ranged from 10 to 30 eV, corresponding to an equilibrium crystal temperature of approximately 135–400 K. The calculation was allowed to continue until the crystal achieved quasithermal equilibrium and then continued for an order of magnitude longer in time to ensure that the observed displacement (or lack of displacement) properly represented the "final" state of the PKA. The simulation time was typically 5 ps. For each direction, the displacement of the PKA from its initial site was determined for several energies resulting in the determination of displacement distance as a function of PKA energy.

III. RESULTS

A. Displacement calculations

As stated earlier, the displacement of a PKA was determined for several initial PKA velocity directions. The primary directions considered in these calculations were within 40° of the $[\bar{1}\,\bar{1}\,\bar{1}]$ (through an open face of the nearest-neighbor tetrahedron) and within 40° of the $[\bar{1}00]$ (i.e., near the center of an edge of the tetrahedron), as indicated in Fig. 1. The directions selected for our calculations [Fig. 1(b)], do not represent a complete covering of the entire triangular region available. The selected points do give a good representation of the central and edge

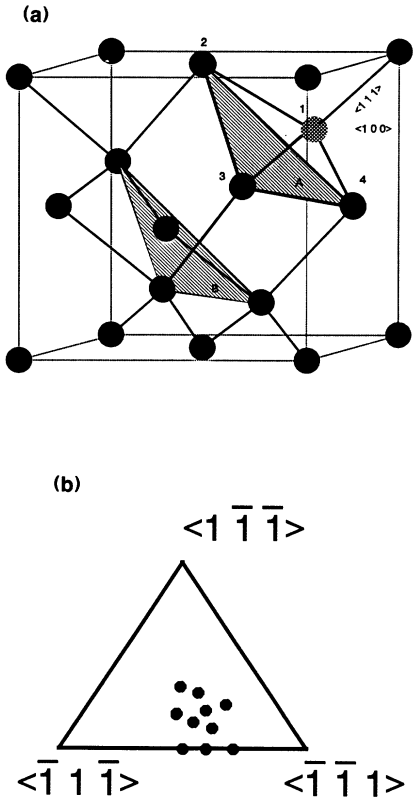

FIG. 1. (a) Silicon unit cell with the PKA shown as the cross-hatched atom 1, which is directed through the shaded triangle A. (b) Tetrahedral face A from (a) showing the crystallographic directions for which Frenkel defect formation was simulated.

center of the triangle, however, and are sufficient to allow a meaningful comparison with experiment. Calculations have been performed for a few points nearer the vertices of the region, but are not reported here since the results lie outside our focus on simple Frenkel defects. In these calculations the strong interaction with the neighboring atoms, which lie at the vertices of the triangle, prevent displacement of the PKA for energies up to ~30–50 eV at which point multiple defects are formed. We do not discuss these events further here.

Plotted in Figs. 2(a), 2(b), and 2(c), respectively, are the total crystal energy, potential energy, and kinetic energy versus time elapsed since the initial-energy impulse for an 18.0-eV PKA. The initial PKA velocity vector for these calculations was in the [0.8447, 0.4744, 0.2476] direction. The *magnitude* of the distance (range) of the PKA from its initial position versus elapsed time is plotted in Fig. 2(d). The range is seen to rapidly increase to approximately 3.5 Å during the first few hundred femtoseconds of the motion, but the PKA soon returns to the vicinity of its original position where small-amplitude vibratory motion ensues. Due to the thermal vibrations excited in the lattice by the initial-energy impulse, the PKA only infrequently visits its precise initial location (i.e., range equal to zero). However, we point out that although the range tends to maintain a nonzero value, the *vector* displacement of the PKA from its initial location averages zero.

Figures 3(a)–3(d) show results similar to those in Fig. 2, but for an initial PKA energy of 25.0 eV. The range of the atom from its equilibrium site is shown in Fig. 3(d). In this case, the PKA is initially displaced approximately 5.1 Å, but returns to a distance near 4.5 Å where it remains for the remainder of the calculation (3 ps). Therefore, for this initial velocity direction, no stable displacement results for the 18.0-eV PKA, but an initial energy of 25.0 eV does lead to a relatively long-lived ("stable") Frenkel pair. Calculations of these types were performed as a function of PKA energy with initial velocity vectors in each of the crystallographic directions shown in Fig. 1(b). Precise identification of these vectors is provided in Tables I–III.

The calculations of displacement distance versus PKA energy for the directions shown in Fig. 1 resulted in four basic types of final-average PKA displacement distance versus initial PKA energy curves. These are plotted in Fig. 4. The simplest of these curves (solid curve *A* in the figure) is for the [0.8447, 0.4745, 0.2476]. For initial PKA energies less than 18.1 eV for this direction, the stable displacement distance is zero. At energies higher than 18.1 eV, the magnitude of the final-average PKA displacement is about 4.5 Å. The relative flatness of the curve above 18.1 eV indicates that the crystal configuration for displacement in this direction corresponds to a deep potential well.

The second type of curve (curve *B*) for the [0.6441, 0.6441, 0.4126] direction is similar to curve *A* in that a sharp displacement-threshold energy results in a minimum displacement of 4.5 Å. However, at higher energies, the displacement distance continues to increase with energy, indicating that the configurational potential

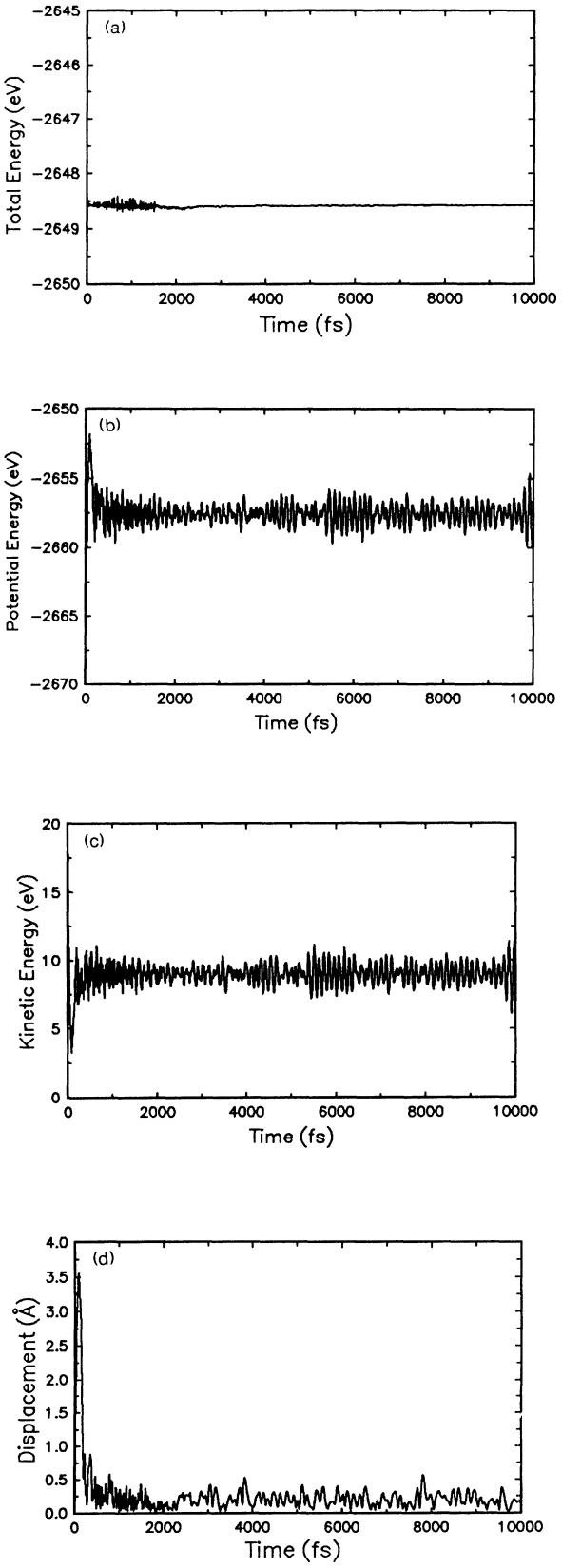

FIG. 2. The (a) total energy, (b) potential energy, (c) kinetic energy, and the (d) displacement distance is shown as a function of time for MD calculation with PKA energy of 18 eV along the ⟨0.8447, 0.4744, 0.2476⟩ direction.

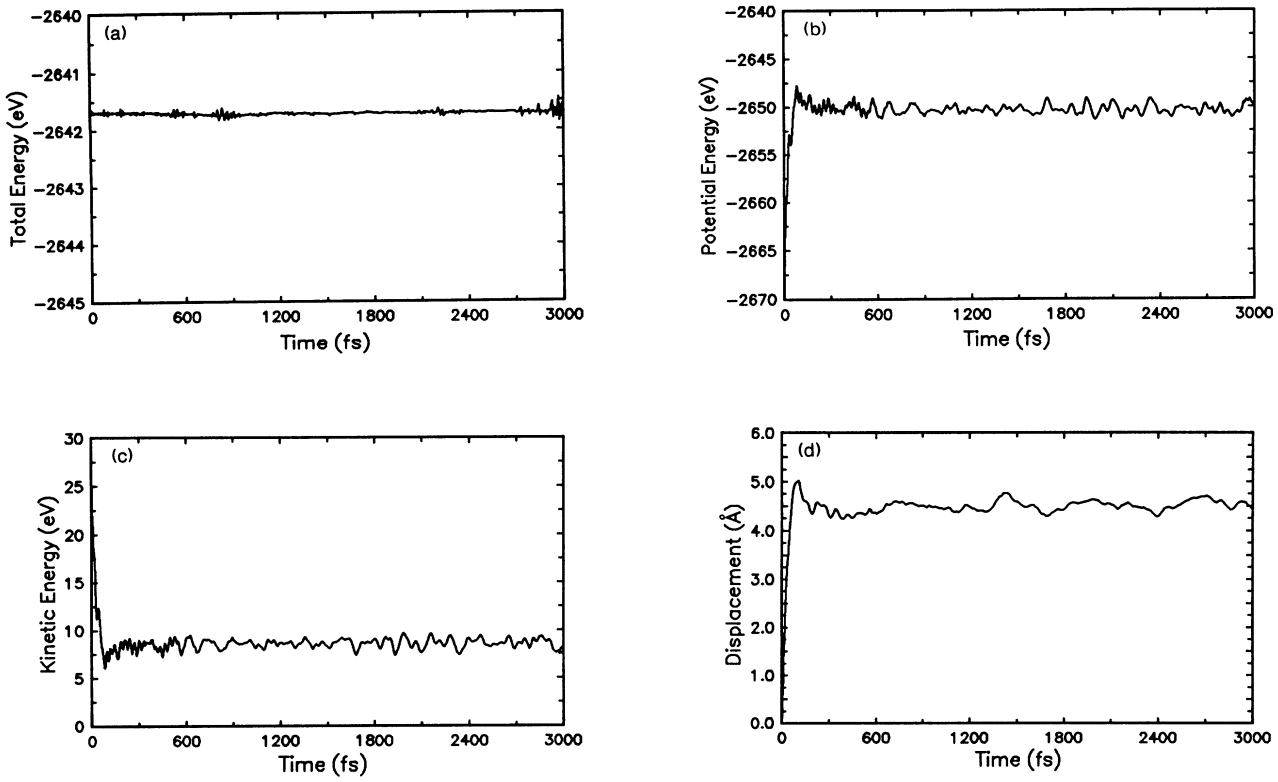

FIG. 3. The (a) total energy, (b) potential energy, (c) kinetic energy, and the (d) displacement distance is shown as a function of time for MD calculation with PKA energy of 25 eV along the ⟨0.8447, 0.4744, 0.2476⟩ direction.

well is not as deep for displacements in this direction. Curve *C*, corresponding to the [0.9848, 0.1228, 0.1228] direction, shows two distinct displacement distances. The first is at approximately 2.3 Å from the initial PKA site. Recoil energies in the range of 10.6–17 eV result in a displacement of this distance (a close Frenkel pair). PKA energies of 18 eV and more result in a displacement of least 4.5 Å (an extended Frenkel pair). In this direction there is evidently a fairly deep well at 2.3 and at 4.5 Å.

The final type of curve (curve *D*) for the [0.902, 0.3364, 0.0535] direction is the most complex case. For PKA energies in the range 20–22 eV, there is a plateau at 2.7 Å similar to that at 2.3 Å for the [0.9848, 0.1228, 0.1228] direction. For energies greater than 22 eV, the PKA is displaced approximately 4.5 Å. We have also observed above-threshold recombination events in the vicinity of 25 eV for this direction, a type of behavior previously seen by King and Benedek[5] in MD calculations for Cu. We find these above-threshold recombination events to be the fortuitous result of dynamic correlations in atomic motion at low initial temperatures. This concept was verified by raising the initial crystal temperature slightly (to 50 K), which resulted in the elimination of all such events (see filled circle in Figs. 4 and 9).

B. Formation energies

Formation energies were calculated for a few representative directions for both close and extended Frenkel pairs.[26] These results are compiled in Table I. The for-

TABLE I. Formation energies of displacement defects.

Direction	PKA energy (eV)	Displacement (Å)	Formation energy (eV)
[0.9962, 0, 0.0872]	15.0	2.25	5.8
[0.9397, 0.2418, 0.2418]	15.0	2.28	5.9
[0.6108, 0.6108, 0.5039]	15.0	4.50	7.8
[0.7041, 0.7041, 0.0915]	20.0	4.51	7.7
[0.9962, 0, 0.0872]	20.0	4.47	8.2
[0.9397, 0.2418, 0.2418]	22.0	4.37	8.4

TABLE II. Calculated bulk displacement-threshold energies for displacement only outside nearest-neighbor tetrahedron.

No.	Direction [$hk1$]	θ,ϕ referenced to [$\bar{1}\bar{1}\bar{1}$] (deg)		θ,ϕ referenced to [$\bar{1}00$] (deg)		E_d (eV)
1	[$\bar{1}\bar{1}\bar{1}$]	0	0	54.75	90.00	11.4
2	[$\bar{0}.7041$, $\bar{0}.7041$, $\bar{0}.0915$]	30.00	0	45.24	52.42	18.3
3	[$\bar{1}00$]	54.74	60.00	0	0	10.1
4	[$\bar{0}.9397$, $\bar{0}.2418$, 0.2418]	57.14	35.97	20.00	0	12.5
5	[$\bar{0}.9402$, $\bar{0}.3364$, $\bar{0}.0535$]	45.07	37.07	19.91	51.50	18.6
6	[$\bar{0}.8447$, $\bar{0}.4745$, $\bar{0}.2476$]	25.23	37.90	32.36	79.72	18.1
7	[$\bar{0}.9434$, $\bar{0}.3070$, $\bar{0}.1258$]	37.39	47.82	19.37	76.41	16.6
8	[$\bar{0}.8881$, $\bar{0}.3251$, $\bar{0}.3251$]	27.37	60.00	27.37	90.00	19.1
9	[$\bar{0}.6441$, $\bar{0}.6441$, $\bar{0}.4126$]	10.90	0	49.90	82.79	12.1
10	[$\bar{0}.9848$, $\bar{0}.1228$, $\bar{0}.1228$]	55.35	47.82	10.00	0	10.6

mation energies of defects with the PKA located in similar interstitial sites were very close (within 0.2 eV). The first two entries in Table I are for interstitials located approximately one interatomic bond length from the vacancy in a ⟨100⟩ split interstitial configuration (i.e., for the first entry, atom 1 has moved through tetrahedral face A in Fig. 1 and forms a [001] split interstitial with atom 2; see Fig. 1). The third and fourth entries in Table I are for the PKA located in a tetrahedral interstitial site. For example, the third entry corresponds to atom 1 moving through tetrahedral faces A and B to come to rest in the tetrahedral site at the opposite corner of the unit cell. Referring again to Fig. 1, the final two entries in Table I are for cases where the PKA has traveled almost horizontally across the unit cell through face A to form ⟨100⟩ split interstitials with atoms in the neighboring cell. The formation energies for these vacancy-interstitial (Frenkel-pair) defects are seen to range from about 6 eV for the closer pairs to near 8 eV for the more distant pairs.

C. Displacement-threshold energies

Collected in Table II are our calculated values for E_d for the ten different crystallographic directions shown in Fig. 1(b). The values listed in Table II were obtained using the simple displacement criterion, which requires only that the PKA be outside its original tetrahedron of nearest neighbors as the disturbed crystal comes into quasithermal equilibrium.

Our discussion of Fig. 4 and the calculated formation energies in Table I indicate, however, that more stable defects are formed when displacements to ~ 4.5 Å occur. Accordingly, we have calculated a second set of displacement-threshold energies in which the defect production criterion requires that the "final" vacancy-interstitial separation be greater than $0.75a$, i.e., > 4.1 Å. Results of these calculations are collected in Table III. We point out that for these calculations we substituted initial PKA velocity direction numbers 11 and 12 in Table III in place of direction numbers 1 and 3 in Table

TABLE III. Bulk displacement-threshold energies for displacement beyond $\frac{3}{4}$ of a cubic unit-cell width.

No.	Direction [$hk1$]	θ,ϕ Referenced to [111] (deg)		θ,ϕ Referenced to [100] (deg)		E_d (eV)
1	[$\bar{0}.6108$, $\bar{0}.6108$, $\bar{0}.5039$]	5.00	0	52.35	86.83	11.5
2	[$\bar{0}.7041$, $\bar{0}.7041$, $\bar{0}.0915$]	30.00	0	45.24	52.42	18.3
3	[$\bar{0}.9962$, 0.0, $\bar{0}.0872$]	51.28	64.53	5.00	0	17.0
4	[$\bar{0}.9397$, $\bar{0}.2418$, 0.2418]	57.14	35.97	20.00	0	21.0
5	[$\bar{0}.9402$, $\bar{0}.3364$, $\bar{0}.0535$]	45.07	37.07	19.91	51.50	22.0
6	[$\bar{0}.8447$, $\bar{0}.4745$, $\bar{0}.2476$]	25.23	37.90	32.36	79.72	18.1
7	[$\bar{0}.9434$, $\bar{0}.3070$, $\bar{0}.1258$]	37.39	47.82	19.37	76.41	18.0
8	[$\bar{0}.8881$, $\bar{0}.3251$, $\bar{0}.3251$]	27.37	60.00	27.37	90.00	19.2
9	[$\bar{0}.6441$, $\bar{0}.6441$, $\bar{0}.4126$]	10.90	0	49.90	82.79	12.2
10	[$\bar{0}.9848$, $\bar{0}.1228$, $\bar{0}.1228$]	55.35	47.82	10.00	0	18.0

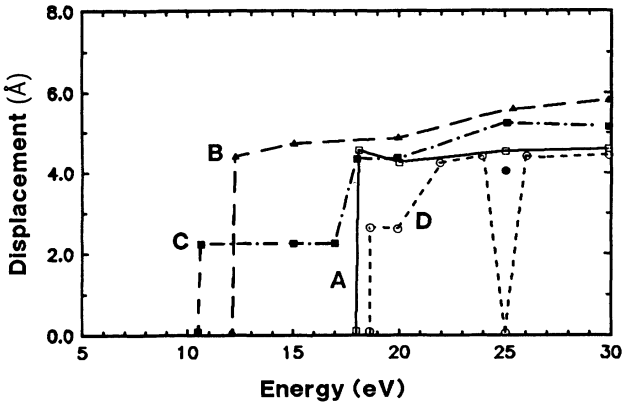

FIG. 4. Four typical types of calculated displacement distance vs PKA energy curves for the directions indicated for the ⟨111⟩ direction [Eq. (9)]: *A* is the [0.8447, 0.8447, 0.2476], *B* is the [0.6441, 0.6441, 0.4126], *C* is the [0.9848, 0.1228, 0.1228], and *D* is the [0.9402, 0.3364, 0.0534].

II. The change of initial velocity direction by 5°, which results from this substitution, was required to avoid direct, head-on collisions between the PKA and lattice atoms lying at a distance 5.3–5.4 Å in the original direction numbers 1 and 3.

D. Analytical expressions for describing crystal anisotropy

In order to provide a more general description of our displacement-threshold-energy results, and to facilitate comparison with experimental data, we provide analytical expressions for the angular dependence of E_d near the two crystallographic directions ⟨111⟩ (through the open face of the nearest-neighbor tetrahedron) and ⟨100⟩. For polar angle θ measured from the ⟨111⟩, $E_d(\theta,\phi)$ may be expanded as

$$E_d(\theta,\phi)=\sum_{n=0}^{\infty}\sin^{3n}\theta\cos(3n\phi)\sum_{k=0}^{\infty}Q_{2k}^{n}\sin^{2k}\theta\ , \tag{1}$$

where the Q_{2k}^{n} are expansion coefficients and the threefold symmetry in ϕ, the azimuthal angle around ⟨111⟩, is explicit in the expression. A vector to one of the nearest-neighbor lattice sites [atoms 2, 3, or 4 in Fig. 1(a)] determines the reference for which $\phi=0$. For values of θ near ⟨111⟩, Eq. (1) can be approximated by

$$E_d=Q_0^0+Q_2^0\sin^2\theta+Q_0^1\sin^3\theta\cos3\phi+Q_4^0\sin^4\theta\ , \tag{2}$$

where terms of order $\sin^5\theta$ and higher have been neglected.

Equation (2) provides an expression for $E_d(\theta,\phi)$ accurate to order $\sin^4\theta$, the coefficients of which can be evaluated from our molecular-dynamics calculations of E_d for several directions near ⟨111⟩. Averaging Eq. (2) over a cone of angular radius θ_m yields

$$\langle E_d\rangle=Q_0^0+\frac{Q_2^0}{3(1-\cos\theta_m)}[2-\cos\theta_m(\sin^2\theta_m+2)]+\frac{Q_4^0}{5(1-\cos\theta_m)}\{\tfrac{4}{3}[2-\cos\theta_m(\sin^2\theta_m+2)]-\sin^4\theta_m\cos\theta_m\}\ . \tag{3}$$

Similar expansions may be written for other symmetry directions, in particular for the ⟨100⟩. For polar angle θ measured from the ⟨100⟩, we expand $E_d(\theta,\phi)$,

$$E_d(\theta,\phi)=\sum_{l=0}^{\infty}\sin^{2l}\theta\cos2l\phi\sum_{k=0}^{\infty}P_{2k}^{l}\sin^{2k}\theta\ , \tag{4}$$

where the P_{2k}^{n} are expansion coefficients for this case, and the twofold symmetry in ϕ, the azimuthal angle about ⟨100⟩, is explicit in the expression. The reference for $\phi=0$ is set by a vector to one of the two nearest-neighbor tetrahedron sites (here for direction $[\bar{1}00]$ from atom 1 this vector is from atom 1 to atoms 2–3). For values of θ near $[\bar{1}00]$, Eq. (4) is approximated by

$$E_d(\theta,\phi)=P_0^0+P_2^0\sin\theta+P_0^l\sin^2\theta\cos2\phi\ , \tag{5}$$

where terms of order $\sin^4\theta$ and higher have been neglected.

Similar to Eq. (2), Eq. (5) provides an approximate expression for $E_d(\theta,\phi)$ accurate to order $\sin^3\theta$, the coefficients of which can be evaluated from molecular-dynamics calculations of E_d for several directions near ⟨100⟩. An average of Eq. (5) over a cone of angular radius θ_m yields

$$\langle E_d\rangle=P_0^0+\frac{P_2^0}{3(1-\cos\theta_m)}[2-\cos\theta_m(\sin^2\theta_m+2)]\ . \tag{6}$$

E. Close Frenkel-pair formation

As noted earlier, for the PKA energy range considered here, there are two typical PKA displacement distances that correspond to close and extended Frenkel pairs (see Fig. 4). The criterion used for the displacement-threshold energy for close Frenkel-pair formation is that the crystal reaches quasithermal equilibrium with the thermalized PKA outside of its original tetrahedron of nearest neighbors. The MD values for E_d based on this criterion in Table II with $\theta<40°$ were used to fit the expansion coefficients of the truncated series about the ⟨111⟩ [Eq. (2)]. A least-mean-square error fit of Eq. (2) to these data points results in

$$E_d(\theta,\phi)=11.4+80.9\sin^2\theta-5.04\sin^3\theta\cos3\phi-194.6\sin^4\theta\ , \tag{7}$$

where the coefficient values are in eV. Equation (7) is only valid for $\theta<40°$ since the small-angle expansion of Eq. (1) was fit to data with θ in this range. Predicted values for E_d from Eq. (7) are compared with our initial MD values in Table IV. The rms deviation of the analytic results from our molecular-dynamics result is 1.2 eV, and the maximum relative difference between a value calculated with the MD code and the value predicted by the analytic expansion is 15%.

Equation (7) is plotted in Fig. 5 for $\theta<40°$ and $0<\phi<360°$. The variables x and y of the plot are related to θ and ϕ by $x=\sin\theta\cos\phi$ and $y=\sin\theta\sin\phi$. The figure shows the dependence of E_d on azimuthal angle to be small, as is expected from the coefficients in Eq. (7); also, E_d exhibits a maximum value at an intermediate value of

TABLE IV. Close Frenkel pairs: Comparison of molecular-dynamics values E_d with those obtained from the analytic expressions of Eqs. (7) and (8).

MD calculated value (eV)	⟨111⟩ expansion Analytic value (eV)	⟨111⟩ expansion Δ[a] (eV)	⟨100⟩ expansion Analytic value (eV)	⟨100⟩ expansion Δ[a] (eV)
11.4	11.4	0.0	b	
18.3	18.8	−0.5	b	
10.1	b		10.1	0.0
12.5	b		14.1	−1.6
18.6	b		14.2	4.4
18.1	19.8	−1.7	20.6	−2.5
16.6	15.7	0.9	14.1	2.5
19.1	20.3	−1.2	17.8	1.3
12.2	14.0	−1.8	b	
10.6	b		11.1	−0.5

[a](MD value) − (analytic value).
[b]The analytic expression is not valid for these directions ($\theta > 40°$).

θ between 0 and 40°. For the coefficients of Eq. (7), the maximum in E_d occurs at $\theta_0(\phi)$, where $\sin\theta_0 = 0.456 - 0.010\cos 3\phi$, or $\theta_0 \sim 27°$, and $E_d(\theta_0) \sim 19.8 - 0.5\cos 3\phi$.

A similar fit of Eq. (5) to the MD values shown in Table II for those points for which $\theta < 40°$ allows the evaluation of the expansion coefficients of the truncated series in the ⟨100⟩ [Eq. (5)]. The resultant equation is

$$E_d(\theta,\phi) = 10.1 + 35.27\sin^2\theta - 2.605\sin^2\theta\cos 2\phi \ , \qquad (8)$$

with coefficient values again in eV. This equation is also only valid for $\theta < 40°$.

A comparison of the analytic values of E_d calculated from Eq. (8) with the MD value of Table II is given in Table IV. For the valid directions, the rms deviation between analytic and molecular-dynamics results is 2.3 eV with a maximum relative difference between the MD values and the corresponding value predicted by the analytic expression of 24%. Figure 6 shows the three-dimensional plot of E_d about the ⟨100⟩ direction from Eq. (8). The displacement threshold monotonically increases with θ while the dependence on ϕ is slight.

The analytic approximation for the average bulk displacement-threshold energies $\langle E_d \rangle$ [Eqs. (3) and (6)] were used to determine $\langle E_d \rangle$ values for the ⟨111⟩ and ⟨100⟩ with angles θ_m of 30° and 20°, respectively. This resulted in an average bulk displacement energy of 17.5 eV in the ⟨111⟩ direction and 12.2 eV in the ⟨100⟩ direction. Directly, these values will be compared with a model proposed by Hemmet and Stevens[27] (HS), which incorporates these specific averages.

F. Extended Frenkel-pair formation

In contrast to the close Frenkel-pair-formation thresholds analyzed above, extended Frenkel-pair formation is defined with the final location of the PKA at least three quarters of a cubic unit-cell width (~ 4 Å) away from its original site. This definition follows naturally from calculated results such as those shown in Fig. 4. For this case, the MD values of E_d in Table III with $\theta < 40°$ were used to obtain values for the expansion coefficients of the truncated series in the ⟨111⟩ [Eq. (2)]. These extended Frenkel-pair-formation threshold values were not always determined to the same precision as those for a simple displacement from the nearest-neighbor tetrahedron. (The tabulated E_d values without a decimal point in Table III are accurate to ~ 1.3 eV.) The values reported in Table III are the lowest recoil energies that resulted in a PKA-vacancy separation greater than three quarters of a cubic unit-cell width (~ 4 Å). Evaluating the expansion coefficients in Eq. (2) for the data of Table III for ⟨111⟩ for $\theta < 40°$ results in

$$E_d(\theta,\phi) = 10.6 + 64.1\sin^2\theta - 4.54\sin^3\theta\cos 3\phi - 126.9\sin^4\theta \ , \qquad (9)$$

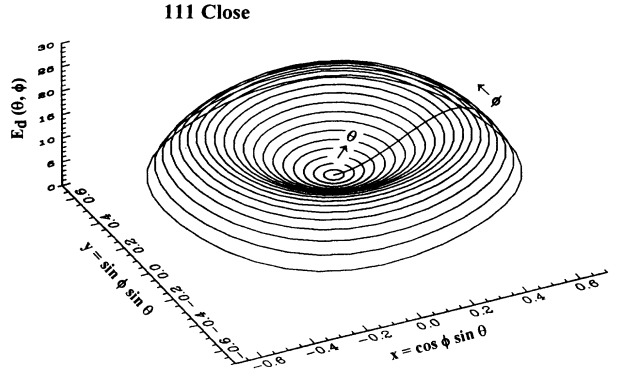

FIG. 5. Analytic representation of the displacement energy E_d about the ⟨111⟩ direction for close displacements [Eq. (7)]. The independent variables x and y for this plot are the indicated functions of θ and φ. Thus, the figure corresponds to a projection onto a (111) plane of the polar plot of the magnitude of E_d on a unit sphere.

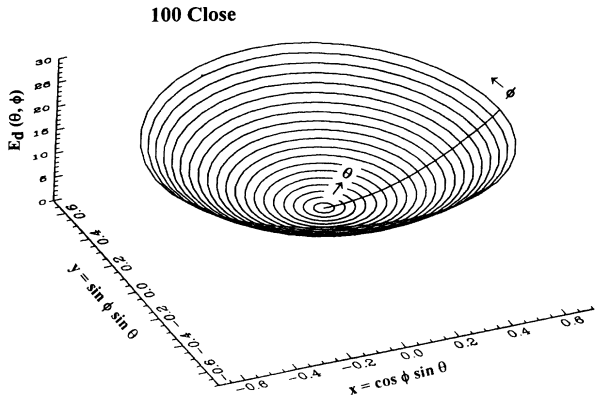

FIG. 6. Analytic representation of the displacement energy E_d for close displacements about the ⟨100⟩ direction [Eq. (8)]. The variables x and y are the indicated functions of θ and φ. Thus, the figure corresponds to a projection onto a (100) plane of the polar plot of the magnitude of E_d on a unit sphere.

with coefficient values in eV. Predicted bulk displacement-threshold energies from Eq. (9) are compared with the MD values in Table V. For these directions, with $\theta < 40°$, the standard deviation of the analytic result from the MD results is 0.9 eV, and the maximum relative difference between a value calculated with the MD code and the corresponding value from the analytic expansion is 9%. A three-dimensional plot of Eq. (19) is given in Fig. 7. The shape of the surface shown in Fig. 7 is qualitatively similar to that given for the near displacement threshold (Fig. 5), but the displacement threshold in Fig. 7 exhibits a weaker dependence on both θ and ϕ. The maximum in E_d occurs now at $\theta_0(\phi)$, where $\sin\theta_0 = 0.503 - 0.013\cos 3\phi$, or at $\theta_0 \sim 30°$, which is little changed from the earlier result for close Frenkel pairs. Also, $E_d(\theta_0) = 18.7 - 0.6\cos 3\phi$.

The MD values in Table III for the ⟨100⟩ are also used to obtain expansion coefficients of the corresponding truncated series in the ⟨100⟩ for those points for which $\theta < 40°$. The resultant approximate equation is

$$E_d(\theta,\phi) = 17.4 + 20.9\sin^2\theta + 15.6\sin^2\theta\cos 2\phi \ , \qquad (10)$$

where the coefficients are in units of eV. Predicted bulk displacement-threshold energies calculated with Eq. (10) are compared with the corresponding MD values in Table V. For those directions with $\theta < 40°$, the standard deviation of the analytic result from the MD result is 1.5 eV and the maximum relative difference between a value determined with the MD code and the value predicted by the analytic expression is 17%.

Equation (10) for the ⟨100⟩ threshold-energy surface is plotted in Fig. 8. In contrast to the other expressions for E_d [Eqs. (7)–(9)], the surface in Fig. 8 exhibits a strong dependence on ϕ with minima for E_d at $\phi = 90°$ and 270° and maxima at 0° and 180°. The maxima correspond to directions lying closest to the two near-neighbor tetrahedron sites on either side of the ⟨100⟩ (see Fig. 1). The average bulk displacement-threshold energies $\langle E_d \rangle$,

TABLE V. Extended Frenkel pairs: Comparison of molecular-dynamics values for E_d with those obtained from the analytic expressions of Eqs. (9) and (10) and values.

	⟨111⟩ expansion		⟨100⟩ expansion	
MD calculated value (eV)	Analytic value (eV)	Δ[a] (eV)	Analytic value (eV)	Δ[a] (eV)
11.5	11.3	0.2	b	
18.3	19.4	−1.1	b	
17.0	b		18.0	−1.0
21.0	b		21.0	0
22.0	b		20.0	2.0
18.1	18.6	−0.5	21.1	−3.0
18.0	19.6	−1.6	19.0	−1.0
19.2	19.8	−0.6	20.3	−1.1
12.2	12.5	−0.3	b	
18.0	b		18.0	0

[a](MD value) − (analytic value).

[b]The analytic expression is not valid for these directions ($\theta > 40°$).

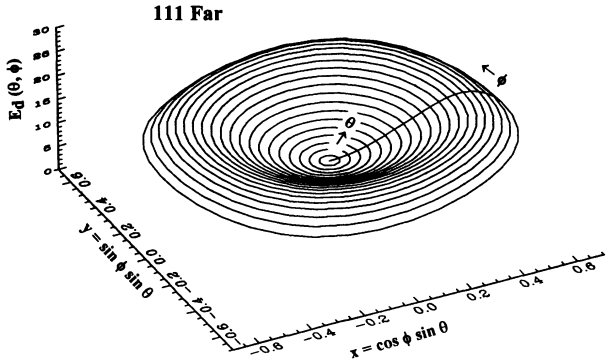

FIG. 7. Same as Fig. 5 for far displacements for the ⟨111⟩ direction [Eq. (9)].

from Eq. (3) for the ⟨111⟩ and Eq. (6) for the ⟨100⟩ for angles θ_m of 30° and 20°, respectively, have been calculated from the numerical coefficients in Eqs. (9) and (10). This resulted in an average bulk displacement energy through the open face of the nearest-neighbor tetrahedron of 16.2 eV along the ⟨111⟩ and 18.6 eV along the ⟨100⟩.

IV. DISCUSSION

A. Formation energies

There seems to be no reliable experimental data on point-defect formation energies,[9,13] but theoretical estimates[28–30] based on the local-density approximation of density-functional theory suggest that for the tetrahedral interstitial 5–6 eV is required while 4–5 eV is required for the hexagonal interstitial. Tersoff has calculated the formation energies for isolated vacancies and interstitials for the potential function utilized in the present calculations.[9] He finds a value of 3.7 eV for the isolated vacancy and values from 3.8 to 5.9 eV for the interstitial, depending on its lattice location, with 4.7 eV for the split interstitial observed in our calculations. Kitabatake and Greene[18] obtain similar values for vacancies and a fairly similar range of values for interstitials near the Si(001)

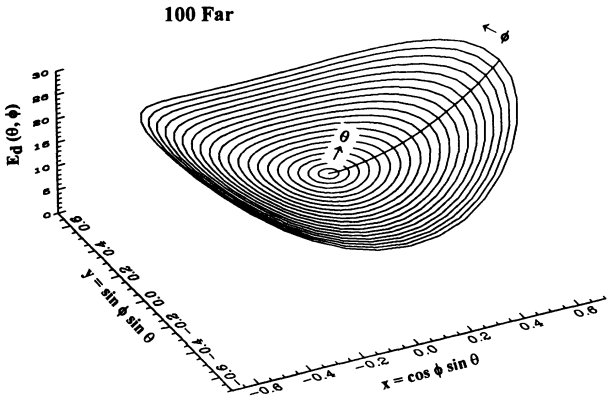

FIG. 8. Same as Fig. 6 for far displacements for the ⟨100⟩ direction [Eq. (10)].

surface, also using the Tersoff potential. We note that with only nearest-neighbor bonding, as is the case for the Tersoff potential used here, the limiting value for the combined formation energies of the isolated vacancy and interstitial should not be greater than twice the cohesive energy of the crystal (9.2 eV here).

The Frenkel-pair formation energies, which we give in Table I, reflect the sum of formation energies for the isolated vacancy and interstitial, plus any interaction energy between the two point defects. The last two entries in the table thus represent essentially isolated point defects since in such case the formation energy should be 8.4 eV (3.7 + 4.7 eV from the discussion above). The first two entries in Table I, in contrast, show a considerable attractive interaction, i.e., $\Delta E \sim 2.5$ eV $= (8.4 - 5.9$ eV). In this latter case, the Frenkel pair is expected to have a limited lifetime due to the attractive force represented by the 2.5 eV of "binding energy."

B. Displacement thresholds

The evaluation of displacement-threshold energies through MD simulation is, in principle, a simple procedure. The calculation is made complicated, however, by the lack of a precise simple definition of just what constitutes a displacement event. We began our investigation of the displacement phenomenon using what we considered to be the simplest possible definition of a displaced atom. That is, when a PKA is displaced outside the tetrahedron of its four initial nearest-neighbor atoms and then comes into quasithermal equilibrium with the surrounding lattice before recombining with the resultant vacancy, a displacement event is said to have occurred. Our calculated $E_d(\theta,\phi)$ surface using this definition does not agree well with the corresponding map extracted by Hemment and Stevens[20,27] from experimental electron-induced radiation damage in silicon.

As indicated above, this simple definition of displacement often leads to close Frenkel pairs. In view of the dependence of Frenkel-pair formation energy on vacancy-interstitial separation, such close pairs are likely to recombine in a time short compared with characteristic measurement times. As a result, closer examination of the details of the displacement processes predicted by our calculations, and as displayed in part in Fig. 4, suggests that a model displacement event should require at least a 4-Å separation of the vacancy and interstitial in order to lead to a stable defect. This new definition which incorporates the notion of defect stability (or lifetime) improves the agreement between our calculations and the analysis of experimental data provided by HS. Discussion of results obtained using each of the displacement models is presented below.

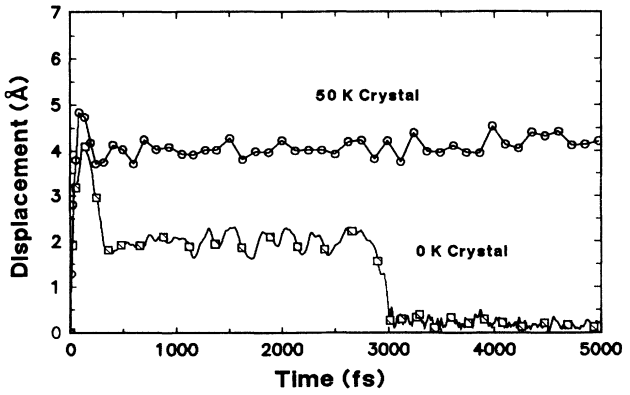

FIG. 9. Comparison of the calculated displacement distance vs time for a 25-eV PKA for an initial crystal temperature of 0 K with the corresponding result for a temperature of 50 K.

1. Close Frenkel-pair formation

Our simplest criterion for atomic displacement in the silicon lattice requires only that the PKA be displaced from the interior of the tetrahedron defined with the four nearest neighbors at its vertices. This definition allows the formation of Frenkel pairs separated by approximately one bulk interatomic bond length, as typified by the first two entries in Table I. These defect pairs, which we label as close Frenkel pairs, probably persist only for a relatively short duration both due to the proximity of the individual defects and to the attractive nature of the accompanying strain field, as indicated by the formation energies of Table I. To verify this we have estimated E_r, the energy barrier to recombination for these close Frenkel pairs, using a simple form of transition-state theory.[15] Our calculations provide an upper bound to E_r of 0.1 eV. At 80 K, the lowest temperature at which experimental measurements have been reported,[27] this value for E_r suggests an average lifetime for these defects less than 0.2 μsec. This result supports our argument that the limited lifetime of these defects has prevented experimental observation of them. Since such energy barriers have been shown to be sensitive to precise details of the potential function (see, e.g., Wang and Rockett[15]), this conclusion should be viewed as tentative.

The anisotropy of the displacement-threshold energy $E_d(\theta,\phi)$, which results from this simple displacement criterion, was analyzed in Sec. III, and average values for E_d, $\langle E_d \rangle$, were obtained for conical regions of 30° and 20° centered on the $\langle 111 \rangle$ and $\langle 100 \rangle$ directions, respectively. These average values for E_d can be directly compared with the HS model[20] developed to explain the anisotropy of the measured electron-induced radiation damage (carrier-removal rates[27,31]) in silicon. For this model HS obtain values of $\langle E_d \rangle(111) = 22$ eV and $\langle E_d \rangle(100) = 26$ eV.[32] In contrast to the results presented by HS, our MD results for $\langle E_d \rangle$ (Sec. III E), based on the simple definition of a displacement event, show a different pattern of anisotropy and are lower than those determined by HS.

The comparison between the anisotropy map obtained in the present work for the formation of close Frenkel pairs and that obtained by HS to explain the observed anisotropy in electron-radiation-damage studies supports the notion that the close paris are short lived. That is, in order to produce Frenkel pairs that are sufficiently stable to lead to measurable radiation damage, the initial vacancy-interstitial pair must be separated by a greater

distance than required by our simple displacement criterion.

2. Extended Frenkel-pair formation

The inconsistencies between our results and those of HS (which show excellent agreement with experimental carrier-removal rates[27,31]), suggested that we examine the energy requirements of the Tersoff potential function for producing extended Frenkel pairs. Typical results from these calculations are shown in Fig. 4 where we have plotted the separation of the PKA and its associated vacancy as a function of PKA initial energy, for four initial PKA momentum directions. The plotted data clearly show that for the PKA energy range considered, two distinct vacancy-interstitial separation distances are favored. The first distance, approximately 2.3 Å, or a bulk interatomic bond length, corresponds to Frenkel pairs with formation energy ~6 eV (Table I). The second distance, approximately $\frac{3}{4}$ of the width of the cubic unit cell, corresponds to Frenkel pairs with ~8-eV formation energy (Table I), and thus to nearly isolated vacancy-interstitial pairs.

The E_d surface obtained when we require this second distance as the criterion for stable displacement was described in Sec. III. The average values obtained from this map for comparison with HS are $\langle E_d \rangle(111)=16.2$ eV and $\langle E_d \rangle(100)=18.6$ eV. These values are still significantly lower than those obtained by HS (particularly in Ref. 27), but the anisotropy is correctly identified and our values change in the proper direction with the consideration of defect separation (stability) factored in.

Although the vacancy and interstitial in the extended Frenkel pairs defined here are almost isolated (from an energetic point of view), nevertheless at a separation of only 4.5 A they are sufficiently close that one can easily imagine rapid recombination through thermal motion. It is not clear, however, that continuing the exercise of increasing the PKA energy and Frenkel-pair separation will lead to better agreement between our MD results and those of HS, particularly since increasing the separation would be expected (at some point) to lead to decreasing anisotropy. The present results may in fact be the best achievable with the Tersoff potential. We are reluctant to proceed further along these lines in any case, since the PKA energies we have already considered are near those which will lead to multiple displacement, thereby further complicating the analysis.

V. SUMMARY

We have presented here dynamical calculations of simple defect production in silicon using a realistic potential-energy function, which reflects both the directional nature of the atomic bonds as well as the forces due to bond bending. The formation energies which we obtain for several configurations of the resultant Frenkel pair provide a measure of the thermal stability of these defects, and suggest a criterion for the production of stable defects. Comparison of our calculated $E_d(\theta,\phi)$ surface for stable defects with the corresponding surface extracted by Hemment and Stevens from experimental electron induced radiation damage shows general agreement in shape, although our values are only about $\frac{2}{3}$ of the experimental ones.

The Tersoff potential was used in the present calculation and the results highlight both the strengths and weaknesses inherent in the use of such potentials and in calculations of this type. Directional effects seem to be faithfully reproduced by our calculations, while absolute values for the displacement energies are underestimated.

ACKNOWLEDGMENTS

This work was performed at Sandia National Laboratories, which is operated by the Department of Energy, under Contract No. DE-AC04-94AL85000.

[1]J. B. Gibson, A. N. Goland, M. Milgram, and G. H. Vineyard, Phys. Rev. **120**, 1229 (1960).
[2]C. Erginsoy, G. H. Vineyard, and A. Englert, Phys. Rev. **133**, A595 (1964).
[3]J. R. Beeler and M. F. Beeler, in *Atomic Collisions in Solids*, edited by S. Datz, B. R. Appleton, and C. D. Moak (Plenum, New York, 1975), Vol. 1, p. 105.
[4]J. R. Beeler, Jr., *Radiation Effects Computer Experiments* (North-Holland, Amsterdam, 1983).
[5]W. E. King and R. Benedek, Phys. Rev. B **23**, 6335 (1981).
[6]F. H. Stillinger and T. A. Weber, Phys. Rev. B **31**, 5262 (1985).
[7]J. Tersoff, Phys. Rev. Lett. **56**, 632 (1986).
[8]J. Tersoff, Phys. Rev. B **37**, 6991 (1988).
[9]J. Tersoff, Phys. Rev. B **38**, 9902 (1988).
[10]J. Tersoff, Phys. Rev. B **39**, 5566 (1989).
[11]R. Biswas and D. R. Hamann, Phys. Rev. B **36**, 6434 (1987).
[12]B. Dodson, Phys. Rev. B **35**, 2795 (1987).
[13]B. C. Bolding and H. C. Andersen, Phys. Rev. B **41**, 10 568 (1990).
[14]See, for example, B. Dodson, Phys. Rev. B **33**, 7361 (1986); K. E. Khor and S. Das Sarma, *ibid.* **36**, 7733 (1987); B. P. Fuesston, R. K. Kalia, and P. Vashishta, *ibid.* **37**, 6297 (1988); E. Blaisten-Barojas and D. Levesque, *ibid.* **34**, 3910 (1986).
[15]See, for example, R. Smith, D. E. Harrison, Jr., and B. J. Garrison, Phys. Rev. B **40**, 93 (1989); J. Wang and A. Rockett, *ibid.* **43**, 12 571 (1991); D. Srivastava and B. J. Garrison, J. Chem. Phys. **95**, 6885 (1991); J. Vac. Sci. Technol. A **8**, 3506 (1990).
[16]M. Kitabatake, P. Fons, and J. E. Greene, J. Vac. Sci. Technol. A **8**, 3726 (1990).
[17]M. Kitabatake, P. Fons, and J. E. Greene, J. Vac. Sci. Technol. A **9**, 91 (1991).
[18]M. Kitabatake and J.E. Greene, J. Appl. Phys. **73**, 3183 (1993).
[19]L. A. Miller, D. K. Brice, A. K. Prinja, and S. T. Picraux, in *Defects in Materials*, edited by P. D. Bristowe, J. E. Epperson, J. E. Griffith, and Z. Liliental-Weber, MRS Symposia Proceedings No. 209 (Materials Research Society, Pittsburgh,

1991), p. 171; L. A. Miller, D. K. Brice, A. K. Pringa, and S. T. Picraux, Radiat. Eff. Defect Solids (to be published).

[20]P. L. F. Hemment and P. R. C. Stevens, in *Radiation Effects in Semiconductors,* edited by F. L. Vook (Plenum, New York, 1968), p. 290.

[21]E. Chason, P. Bedrossian, K. M. Horn, J. Y. Tsao, and S. T. Picraux, Appl. Phys. Lett. **57**, 1793 (1990).

[22]R. S. Averback and M. A. Kirk, in *Surface Alloying by Ion, Electron, and Laser Beams,* edited by L. E. Rehn, S. T. Picraux, and H. Wiedersich (American Society for Metals, Metals Park, OH, 1987), p. 91.

[23]R. G. Elliman, J. S. Williams, W. L. Brown, A. Leiberich, D. M. Maher, and R. V. Knoell, Nucl. Instrum. Methods B **19/20**, 435 (1987).

[24]J. W. Corbett and J.C. Bourgion, in *Point Defects in Solids Volume 2: Semiconductors and Molecular Crystals,* edited by J. H. Crawford, Jr. and L. M. Slifkin (Plenum, New York, 1975).

[25]R. Smith and D. E. Harrison, Jr., Comput. Phys. **3**, 68 (1989).

[26]Frenkel-pair formation energies E_f are defined here as the increase in average potential energy of the computational crystallite due to the creation of a given Frenkel-pair configuration minus the average kinetic energy in the final-state configuration. This definition assumes that the vibrational contribution to the final-state average potential energy is equal to the average final-state kinetic energy, and is precise for the case in which the vibrational motion is simple harmonic in character.

[27]P. L. F. Hemment and P. R. C. Stevens, in *Atomic Collision Phenomena in Solids,* edited by D. W. Palmer, M. W. Thompson, and P. D. Townsend (North-Holland, Amsterdam, 1970), p. 280.

[28]G. A. Baraff and M. Schluter, Phys. Rev. B **30**, 3460 (1984).

[29]Y. Bar-Yam and J. D. Joannopolous, Phys. Rev. Lett. **52**, 1129 (1984).

[30]R. Car, P. J. Kelly, A. Oshiyama, and S. T. Pantelides, Phys. Rev. Lett. **52**, 1814 (1984); **54**, 360 (1985).

[31]I. N. Haddad and P. C. Banbury, Philos. Mag. **14**, 829 (1966); **14**, 841 (1966).

[32]In a later (Ref. 27) more detailed treatment mapping out the E_d surface, HS obtained slightly higher displacement-threshold energies. The anisotropy and other qualitative differences remain the same, however, and no additional insight is provided by the more difficult comparison to the map of Ref. 27.